CHEMISTRY OF MATERIALS
Article

Chem. Mater. **2009,** *21,* 3549–3561 3549
DOI:10.1021/cm900281r

Structure, Conductivity, and Thermal Expansion Studies of Redox Stable Rutile Niobium Chromium Titanates in Oxidizing and Reducing Conditions

Anna Lashtabeg,* Jesus Canales-Vazquez, John T. S. Irvine, and John L. Bradley

School of Chemistry, University of St. Andrews, North Haugh, St. Andrews, Scotland KY16 9ST, U.K.

Received January 29, 2009. Revised Manuscript Received June 16, 2009

Materials from the solid solution with general formula $Ti_{1-2x}Cr_xNb_xO_2$ ($0 < x \leq 0.5$) were synthesised and their structure, conductivity, redox behavior, and thermal expansion studied in air and under reducing conditions of up to 10^{-20} atm $p(O_2)$. Their rutile structure ($P4_2/mnm$) is retained after reduction, though TEM analysis showed that crystallographic shear planes were formed on reduction to accommodate oxygen vacancies. The conductivity of these materials at 900 °C in air was $1.5 - 1.7 \times 10^{-2}$ S cm^{-1}, increasing to > 20 S cm^{-1} in 5% H_2/Ar. The lowest conductivity was observed for samples low in titanium content, indicating that the reduction of Ti^{4+} to Ti^{3+} is primarily responsible for the high electronic conductivity in these materials. All samples showed very slow reduction kinetics, and true equilibrium was not achieved even after > 50 h in flowing 5% H_2/Ar at 900 °C, suggesting that the equilibrium conductivity of these materials at 10^{-20} atm may be significantly higher. Conductivity studies as a function of $p(O_2)$ showed complex redox behavior with indications of a number of step transitions and very slow redox kinetics. The thermal expansion coefficient was in the range of $5.6 \times 10^{-6} - 8.6 \times 10^{-6}$ K^{-1}, which changed little between reduced and fully oxidized samples.

Introduction

Materials for solid oxide fuel cell (SOFC) technology are being intensively investigated world wide in an attempt to extend their operational life to 40 000 h, needed for successful commercialization in residential power type applications. Their high operating temperature, normally 800−1000 °C, causes a number of materials problems, such as long term chemical stability, gas sealing, and mechanical stability of the cell, although high temperature operation is desirable to enhance overall system efficiency especially through combined heat and power operation.

The anode is one of the most important components. To date the state of the art anode is Ni/yttria-stabilized zirconia (YSZ) cermet due to its excellent catalytic properties, high current collection ability, and good chemical and mechanical compatibility with other cell components, namely, the YSZ electrolyte. However, some problems do exist for the Ni-YSZ anode such as long term stability of Ni, which has a low tolerance for sulfur and suffers from carbon deposition when hydrocarbon fuels are used. Additionally, there is a thermodynamic drive for Ni to sinter at these high operating temperatures, which decreases the catalytically active surface area.

To date several approaches are being investigated to address materials problems at high temperatures, and among these are reduction of fuel cell operating temperature with the development of novel electrolytes,[1,2] the development of novel anode materials,[3−9] particularly mixed ionic−electronic conductors,[10,11] microstructure modification,[12−14] and electronic conductors for partial[15] or total[16−18] replacement of nickel. A number of

*Corresponding author. Present address: Australian Institute for Bioengineering and Nanotechnology (AIBN) Building 75 (L5), Cnr of College and Cooper Road, University of Queensland, St. Lucia QLD 4072, Australia. E-mail: a.lashtabeg@uq.edu.au. Telephone: +61 (0)7 3346 3830. Fax: +61 (0)7 3346 3973.

(1) Ishihara, T.; Furutani, H.; Arikawa, H.; Honda, M.; Akbay, T.; Takita, Y. *J. Electrochem. Soc.* **1999**, *146*(5), 1643–1649.
(2) Lacorre, P.; Goutenoire, F.; Bohnke, O.; Retoux, R.; Laligant, Y. *Nature* **2000**, *404*(6780), 856–858.
(3) Ruiz-Morales, J. C.; Canales-Vazquez, J.; Pena-Martinez, J.; Lopez, D. M.; Nunez, P. *Electrochim. Acta* **2006**, *52*(1), 278–284.
(4) Weston, M.; Metcalfe, I. S. *Solid State Ionics* **1998**, *113−115*, 247–251.
(5) Hartley, A.; Sahibzada, M.; Weston, M.; Metcalfe, I. S.; Mantzavinos, D. *Catal. Today* **2000**, *55*(1−-2), 197–204.
(6) Canales-Vazquez, J.; Tao, S. W.; Irvine, J. T. S. *Solid State Ionics* **2003**, *159*(1−2), 159–165.
(7) Hui, S.; Petric, A. *J. Eur. Ceram. Soc.* **2002**, *22*(9−10), 1673–1681.
(8) Ruiz-Morales, J. C.; Canales-Vazquez, J.; Marrero-Lopez, D.; Irvine, J. T. S.; Nunez, P. *Electrochim. Acta* **2007**, *52*(25), 7217–7225.
(9) Huang, Y.-H.; Dass, R. I.; Xing, Z.-L.; Goodenough, J. B. *Science* **2006**, *312*(5771), 254–257.
(10) Steele, B. C. H. *Solid State Ionics* **2000**, *129*(1−4), 95–110.
(11) Steele*, B. C. H. *Solid State Ionics* **2000**, *134*(1−2), 3–20.
(12) Ruiz-Morales, J. C.; Canales-Vazquez, J.; Pena-Martinez, J.; Marrero-Lopez, D.; Irvine, J. T. S.; Nunez, P. *J. Mater. Chem.* **2006**, *16*(6), 540–542.
(13) Badwal, S. P. S.; Drennan, J. *J. Mater. Sci.* **1987**, *22*(9), 3231–3239.
(14) Muller, A. C.; Herbstritt, D.; Ivers-Tiffee, E. *Solid State Ionics* **2002**, *152−153*, 537–542.
(15) Lashtabeg, A.; Irvine, J. T. S.; Feighery, A. *Ionics* **2003**, *9*(3−4), 220–226.
(16) An, S.; Lu, C.; Worrell, W. L.; Gorte, R. J.; Vohs, J. M. *Solid State Ionics* **2004**, *175*(1−4), 135–138.
(17) Costa-Nunes, O.; Gorte, R. J.; Vohs, J. M. *J. Power Sources* **2005**, *141*(2), 241–249.
(18) Tsipis, E. V.; Kharton, V. V.; Frade, J. R. *J. Eur. Ceram. Soc.* **2005**, *25*(12), 2623–2626.

Published on Web 07/20/2009

comprehensive review articles have been published recently detailing progress in these areas.[19−23]

A potential replacement for Ni in the cermet, or an alternative anode current collector, must display suitable properties, such as high electronic conductivity, chemical and mechanical compatibility with other cell components, and in the case of total replacement a catalytic activity towards the oxidation of hydrogen or hydrocarbons. Many of the novel mixed oxide anode materials such as $Sr_2MgMoO_{6-\delta}$,[9] $La_{0.75}Sr_{0.25}Cr_{0.5}Mn_{0.5}O_{3-\delta}$,[24] or substituted $SrTiO_3$[25−27] require the use of an additional current collector, such as Cu,[8] because of their low electronic conductivity.

As a result of their high electronic conductivity, niobia based rutile materials have been considered as potential candidates for partial replacement of Ni in the Ni/YSZ cermet anode.[15] In a previous study our group investigated the potential of Nb_2TiO_7 to be used as a current collector.[15] Although this material showed a very high electronic conductivity of 100−300 S cm^{-1} at 900 °C in 5% H_2/Ar atmosphere, it had a very low thermal expansion coefficient (TEC) of 2.38×10^{-6} K^{-1} (300−900 °C) in air and 3.21×10^{-6} K^{-1} (300−900 °C) in 5% H_2/Ar, when reduced to $Nb_{1.33}Ti_{0.67}O_4$. Doping with Fe_2O_3 increased the thermal expansion coefficient to $>6 \times 10^{-6}$ K^{-1};[15] however, it did not solve the problem of a large thermal expansion mismatch between the oxidized (2×10^{-6} K^{-1}) and the reduced sample (6×10^{-6} K^{-1}). The large mismatch in the TEC is principally due to the difference in structure between the reduced tetragonal rutile structure with a fairly rigid covalent framework and the oxidized monoclinic structure with additional oxygen that is more able to relieve distortion on increase of temperature. In the anode the low expansion can cause problems with cracking, as one of the important mechanical properties in a current collector is the thermal expansion coefficient, and the candidate must adequately match the other components of the cermet, that is, YSZ. The thermal expansion of the Ni-YSZ cermet is 12×10^{-6} K^{-1}; hence, other components need to be within 20% of this value to be mechanically compatible at 800 °C for 40 000 h, and the thermal expansion of nickel metal itself is 16.9×10^{-6} K^{-1}.

The difference in the electronic conductivities of Nb_2TiO_7 ($4.1 \pm 0.5 \times 10^{-3}$ S cm^{-1} in air at 900 °C) and its reduced counterpart, $Nb_{1.33}Ti_{0.67}O_4$, fueled further interest in this material. Nb_2TiO_7 has a complicated structure with a monoclinic unit cell ($C2/m$), with a = 20.36 Å, b = 3.80 Å, c = 11.89 Å, and β = 120.19°,[15] where Ti^{4+} and Nb^{5+} both occupy the same crystallographic site,[28,29] as expected due to their similar ionic radii (0.60 Å and 0.64 Å respectively), and both cations co-ordinate oxygen predominantly in octahedra. The two kinds of metal atoms are thus disordered, and the average population of any one site is 1/3Ti and 2/3Nb. The reduction of Nb_2TiO_7 produces a double rutile-type structure of stoichiometry $Nb_{1.33}Ti_{0.67}O_4$ similar to NbO_2. The structure is tetragonal ($P4_2/mnm$), with a unit cell of a = 4.76 Å and c = 3.00 Å.

In NbO_2, $Nb_{1.33}Ti_{0.67}O_4$, and other similar niobium based materials, high conductivity is due to the edge sharing of NbO_6 octahedra along the c-axis, producing Nb−Nb metal bond overlap with an inter-metallic distance of 3 Å. This high electronic conductivity is facilitated by the edge sharing octahedra along the c-axis and is therefore an important structural feature to consider when looking for similar niobium based materials. The rutile structure based on Nb−Nb metal bonding overlap will thus produce materials of higher electronic conductivity.

In the search for a niobium based material which has a rutile structure in both oxidizing and reducing atmospheres, the $Nb_xM_x^{III}Ti_{1-2x}O_2$ series were encountered. $Nb_xM_x^{III}Ti_{1-2x}O_2$ (M = Al, Cr, or Fe) solid solution materials were first synthesised and characterized by Tena et al,[30] who found that these materials crystallized in air with a rutile structure, space group $P4_2/mnm$, that is, similar to that of $Nb_{1.333}Ti_{0.667}O_4$. They did not, however, report the structure in reducing conditions, the conductivity of these samples, or their thermal expansion characteristics.

In looking at niobium based rutile materials for use as a current collector in the anode of SOFCs, we investigated whether the $Ti_{1-2x}Cr_xNb_xO_2$ series would show a similarly high electronic conductivity to $Nb_{1.333}Ti_{0.667}O_4$ under the reducing conditions encountered at the anode and examined their thermal expansion characteristics and structure changes.

Experimental Section

The samples of $Ti_{1-2x}Cr_xNb_xO_2$ are readily prepared by pressing mixed stoichiometric amounts of metal oxides (Aldrich, 99.9%) into pellets (3 ton/cm^2) and firing in air at 1200−1400 °C for 72 h with intermediate regrinding. The samples were seen to change from the green color of Cr_2O_3 to dark red or purple on a single 24 hour firing at 1200 °C and remained dark red or purple on all subsequent firing. Prior to XRD, TEM, TEC, and TGA analysis, portions of the samples were pre-reduced at 1000 °C in flowing 5% H_2/Ar for 48 h. The samples were reduced in situ during the four-terminal

(19) Gorte, R. J.; Vohs, J. M. *J. Catal.* **2003**, *216*(1−2), 477–486.
(20) Gorte, R. J.; Vohs, J. M.; McIntosh, S. *Solid State Ionics* **2004**, *175* (1−4), 1–6.
(21) Steele, B. C. H. *Solid State Ionics* **1996**, *86-88*(Part 2), 1223–1234.
(22) Zhu, W. Z.; Deevi, S. C. *Mater. Sci. Eng. A* **2003**, *362*(1−2), 228–239.
(23) Lashtabeg, A.; Skinner, S. J. *J. Mater. Chem.* **2006**, *16*(31), 3161–3170.
(24) Tao, S. W.; Irvine, J. T. S. *Nat. Mater.* **2003**, *2*(5), 320–323.
(25) Ruiz-Morales, J. C.; Canales-Vazquez, J.; Savaniu, C.; Marrero-Lopez, D.; Zhou, W. Z.; Irvine, J. T. S. *Nature* **2006**, *439*(7076), 568–571.
(26) Ruiz-Morales, J. C.; Canales-Vazquez, J.; Savaniu, C.; Marrero-Lopez, D.; Nunez, P.; Zhou, W. Z.; Irvine, J. T. S. *Phys. Chem. Chem. Phys.* **2007**, *9*(15), 1821–1830.
(27) Ovalle, A.; Ruiz-Morales, J. C.; Canales-Vazquez, J.; Marrero-Lopez, D.; Irvine, J. T. S. *Solid State Ionics* **2006**, *177*(19−25), 1997–2003.
(28) Wadsley, A. *Acta Crystallogr.* **1961**, *14*(6), 660–664.
(29) Gasperin, M. *J. Solid State Chem.* **1984**, *53*(1), 144–147.
(30) Tena, M. A.; Escribano, P.; Monros, G.; Carda, J.; Alarcon, J. *Mater. Res. Bull.* **1992**, *27*(11), 1301–1308.

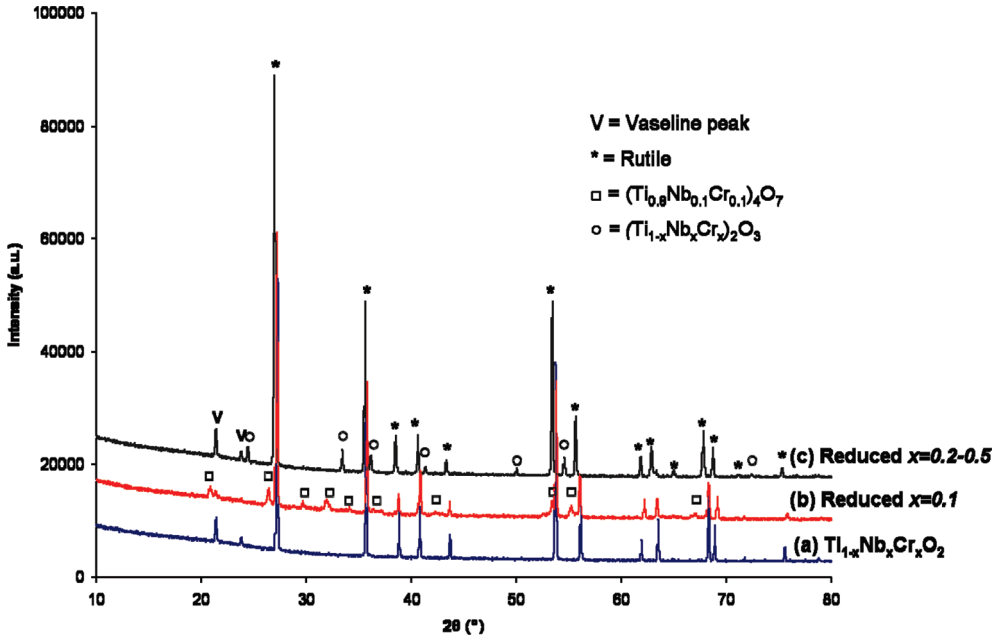

Figure 1. X-ray powder diffraction pattern of (a) oxidized and (b, c) reduced $Ti_{1-2x}Cr_xNb_xO_2$; V is sample mounting peak.

DC measurements and conductivity studies at 900 °C in flowing 5% H_2/Ar. All reduced samples were dark navy blue in color.

Phase purity was checked using a STOE Stadi-P diffractometer using Cu $K\alpha_1$ radiation, (stepwidth 0.02°, 10 s per step), and the unit cell parameters were determined through Rietveld refinement using Topas Academic V4.1. TEM studies were performed on a Jeol JEM 2011 electron microscope operating at 200 kV and equipped with a double tilt (±20°) sample holder. The specimens were prepared by depositing a few drops of a suspension of very fine ceramic powder in acetone onto a perforated C-coated Cu grid. Thermogravimetric analysis was performed using a RheoTherm TGA 1000M+ in flowing air, 20 mL/min, on pre-reduced samples with the temperature increasing from room temperature at a rate of 5 °C/min up to 900 °C, holding at temperature for 60 minutes, after which time no further weight change was observed, and then a cooling rate of 5 °C/min.

Thermal expansion studies were performed in flowing air for samples made in air and in flowing 5% H_2/Ar on pre-reduced samples. The measurements were taken with a Netzsch dilatometer Dil 402C. The change in the sample length is measured via the pushrod by the linear variable displacement transducer, LVDT-System, which in turn is positioned in the cold part of the system. The expansion of the alumina sample holder and other alumina components is corrected for by a calibration correction, from a blank measurement using an alumina standard (Multilab 99.7% purity) of length that matches the sample to within 10%. Pellets were between 8 and 15 mm in length and 70−90% dense. The blank Al_2O_3 sample was measured in both air and 5% H_2/Ar using the same heating/cooling ramp rates of 5 °C/min as the sample to compensate for any atmosphere and heating effects.

DC electrical conductivity measurements were carried out over a range of temperatures under constant atmosphere of air or 5% H_2/Ar, using the four-terminal DC technique, on pellets with densities between 70 and 90%, using Pt contacts. Two terminal AC impedance spectroscopy was also utilized to measure the conductivity of samples, confirming data from four-terminal DC measurements. The dependence of electrical conductivity upon oxygen partial pressure was investigated by four-terminal DC measurements. An in situ reduction step was performed by slowly leaking 5% H_2/Ar at 900 °C into the chamber and measuring the change in $p(O_2)$ with a YSZ oxygen sensor, using a fine needle valve to control the gas flow, and at $p(O_2) < 10^{-15}$ atm this would take up to 20 h. Once the minimum $p(O_2)$ of $\sim 10^{-19}-10^{-20}$ atm was reached, the samples were left for up to 55 h in flowing 5% H_2/Ar to reach a steady equilibrium conductivity, before closing all gas inlets and sealing the chamber. Oxygen was then allowed to leak slowly into the chamber using a capillary needle valve opening to air. The rate of leak was such that the change in $p(O_2)$ from 10^{-20} to $10^{-0.67}$ atm (air) would take up to 100 h to traverse. Once re-oxidized in situ, the samples would be left in air at 900 °C for a further 48 h to establish their final conductivity after the redox cycle.

Results

X-ray Diffraction. *Oxidized $Ti_{1-2x}Cr_xNb_xO_2$ Samples.* Figure 1a shows a typical rutile XRD pattern for this series of materials prior to reduction. The cations in the $Ti_{1-2x}Cr_xNb_xO_2$ structure, similar to $Nb_{1.333}Ti_{0.667}O_4$, all occupy the same crystallographic site, which may be due to the similar sizes of ionic radii of the cations: 0.61 Å for Cr^{3+}, 0.60 Å for Ti^{4+}, and 0.64 Å for Nb^{5+}. From Rietveld refinement of the profile, the unit cell parameters (Table 1) were found to be in good agreement with those reported by Tena et al.,[30] and the unit cell in the $Ti_{1-2x}Cr_xNb_xO_2$ series is seen to increase with x.

The unit cell parameters a and c change linearly with composition, closely following Vegard's law (Figure 2a,b), which applies to solid solutions formed by random substitution or distribution of ions. Vegard's law is not always obeyed, and departures are seen from linearity, as depicted in Figure 2 for the oxidized $Ti_{1-2x}Cr_xNb_xO_2$ series. This is because Vegard's law assumes that the changes in unit cell parameters with composition are governed solely by the relative size of the atoms or ions that replace each other in a simple substitutional mechanism; thus, the unit cell expands if a small ion is substituted by a larger one and vice

Table 1. Unit Cell, *c*/*a* Ratio, and Thermal Expansion Coefficients of Oxidized $Ti_{1-2x}Cr_xNb_xO_2$ (bold) and of $Ti_{1-2x}Cr_xNb_xO_{2-\delta}$ Reduced at 1000 °C (italic)

sample	*a* (Å)	*c* (Å)	*V* (Å^3)	*c*/*a*	TEC 300−900 °C (× $10^{-6}K^{-1}$)
TiO_2	**4.6001(3)**	**2.9654 (4)**	**62.75**	**0.6447**	**7.14−9.19**[57]
$Ti_{0.8}Cr_{0.1}Nb_{0.1}O_2$	**4.6113(1)**	**2.9748(1)**	**63.257(1)**	**0.6451**	**8.57 ± 0.05**
$Ti_{0.6}Cr_{0.2}Nb_{0.2}O_2$	**4.6218(1)**	**2.9852(1)**	**63.768(1)**	**0.6459**	**7.35 ± 0.05**
$Ti_{0.4}Cr_{0.3}Nb_{0.3}O_2$	**4.6309(1)**	**2.9950(1)**	**64.228(2)**	**0.6467**	**6.65 ± 0.05**
$Ti_{0.2}Cr_{0.4}Nb_{0.4}O_2$	**4.6430(1)**	**3.0070(1)**	**64.821(2)**	**0.6476**	**6.27 ± 0.05**
$Cr_{0.5}Nb_{0.5}O_2$	**4.6492(1)**	**3.0144(1)**	**65.157(2)**	**0.6484**	**6.04 ± 0.05**
$Ti_{0.8}Cr_{0.1}Nb_{0.1}O_{1.90}$	*4.6392(1)*	*2.9840(1)*	*64.222(1)*	*0.6432*	*8.34 ± 0.05*
$Ti_{0.6}Cr_{0.2}Nb_{0.2}O_{1.95}$	*4.6417(1)*	*2.9884(1)*	*64.385(1)*	*0.6438*	*7.19 ± 0.05*
$Ti_{0.4}Cr_{0.3}Nb_{0.3}O_{1.97}$	*4.6712(1)*	*2.9995(1)*	*65.449(1)*	*0.6421*	*6.82 ± 0.05*
$Ti_{0.2}Cr_{0.4}Nb_{0.4}O_{1.98}$	*4.6798(1)*	*3.0060(1)*	*65.830(1)*	*0.6423*	*5.71 ± 0.05*
$Cr_{0.5}Nb_{0.5}O_{1.98}$	*4.6825(1)*	*3.0109(1)*	*66.017(2)*	*0.6430*	*5.57 ± 0.05*

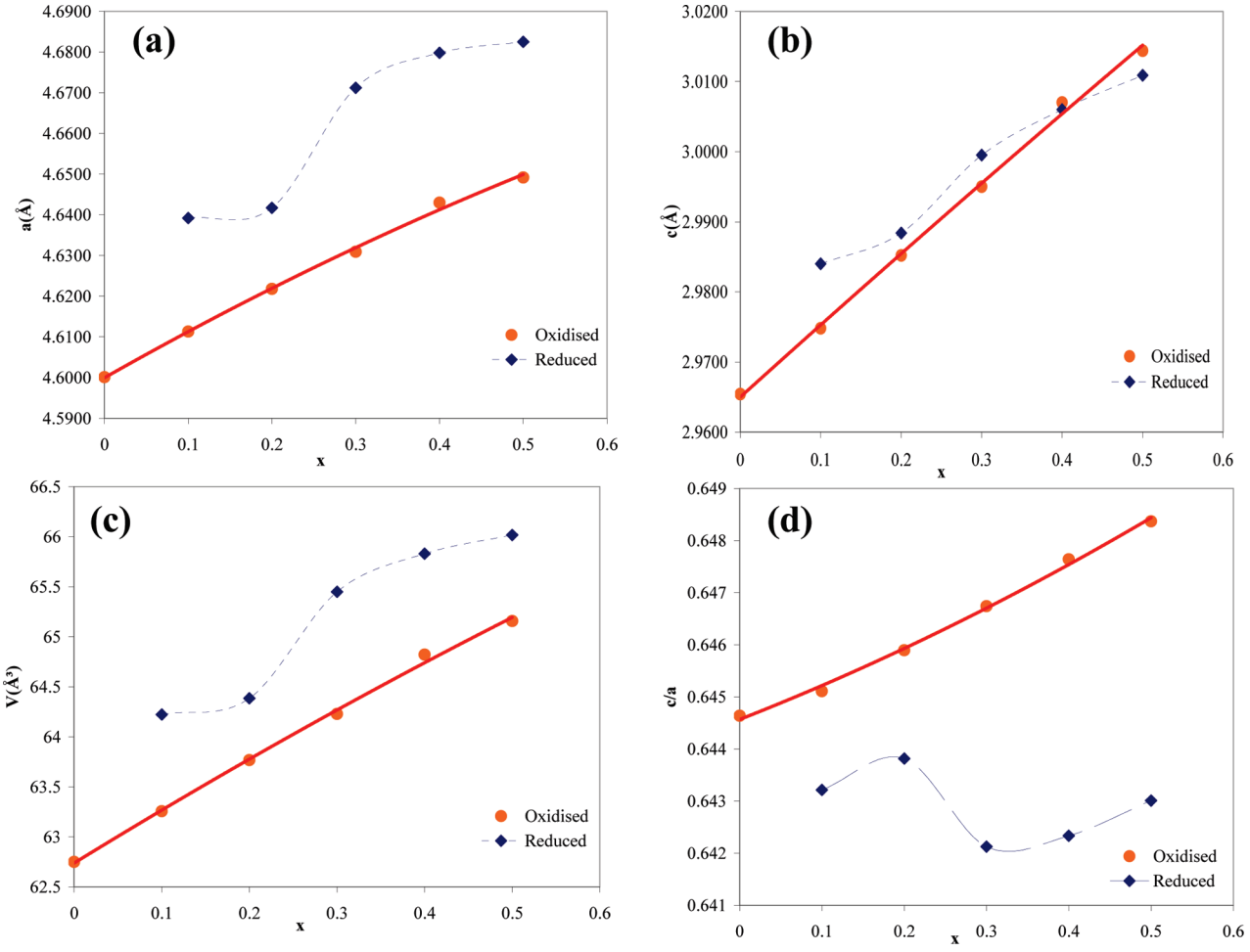

Figure 2. (a) Unit cell parameter *a*, (b) unit cell parameter *c*, (c) unit cell volume, and (d) *c*/*a* ratio as a function of *x* in $Ti_{1-2x}Cr_xNb_xO_2$ made in air (oxidized) or reduced at 1000 °C in 5% H_2/Ar.

versa. In a non-cubic system, such as this one, the expansion or contraction with composition may not be the same for all axes, and sometimes one axis may expand and another contract. The *c*/*a* ratio (Figure 2d, Table 1), increases with *x* for the oxidized sample, indicating that the expansion is greater along the *c* direction than in the *a* direction. From Figure 3, showing a rutile structure, it can be seen that M−M bonds overlap runs in the *c* direction. Replacing the smaller cation, Ti^{4+}, by the larger Nb^{5+} and Cr^{3+} would increase the average inter-atomic distance especially where there is a *d* orbital overlap in the M−M bond, along the *c* axis.

TGA. As a result of the slow reduction rate of the samples, the TGA was performed in flowing air on the pre-reduced samples to determine δ in $Ti_{1-2x}Cr_xNb_xO_{2-\delta}$. As can be seen from Figure 4, the substitution of TiO_2 makes the samples less susceptible to reduction as can be seen in the decrease of oxygen nonstoichiometry, δ. When *x* is 0.1 and 0.2 the values of $\delta = 0.2$ and 0.1, respectively, and this decreases to $\delta = 0.02$ for full TiO_2 substitution in $Cr_{0.5}Nb_{0.5}O_2$. From this trend it can also be assumed that Ti is being reduced preferentially to Cr or Nb. Although the degree of reduction of Nb or Cr requires further study,

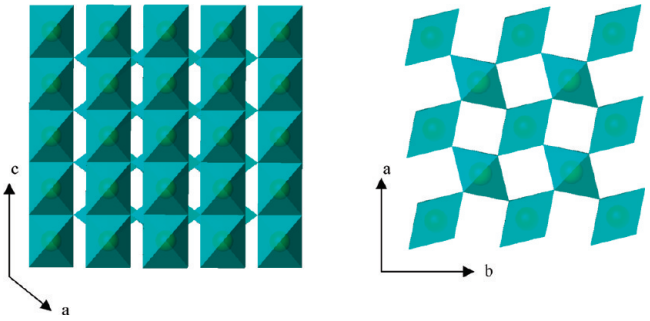

Figure 3. Rutile structure along the *a*/*b* and *c* axes, showing corner and edge sharing octahedra.

Nb_2O_5 is more likely to reduce than Cr_2O_3; thus, it can be assumed that in the $Cr_{0.5}Nb_{0.5}O_2$ composition it is the niobium ion that undergoes reduction.

Reduced Samples. Figure 1b,c show the XRD pattern for the reduced samples, $Ti_{1-2x}Cr_xNb_xO_{2-\delta}$. The XRD pattern of the reduced samples consists of the main rutile phase and additional peaks corresponding to a secondary reduced phase. The cell parameters have been refined and are shown in Table 2. In the titanium rich phase, $x = 0.1$, $Ti_{0.8}Cr_{0.1}Nb_{0.1}O_{1.90}$, the secondary phase corresponds to a Ti_4O_7 equivalent Magneli phase. In samples with $x = 0.2-0.5$, the additional phase correspond to the Ti_2O_3 equivalent phase. Reducing rutile TiO_2 under the same conditions produces a range of Magneli phases, Ti_nO_{2n-1}, with $n = 4-10$, and this is consistent with other studies into the reduction behavior of TiO_2.[31−33] It is worth noting that such phases may typically exist as shear planes or domains rich in shear planes within the main phase crystals. In contrast to $x = 0.1$, only one Magneli phase is seen for $T_{i0.8}Cr_{0.1}Nb_{0.1}O_2$, and only the rhombohedral Ti_2O_3 type phase is seen for the other $Ti_{1-2x}Cr_xNb_xO_{2-\delta}$ samples, $x = 0.2-0.5$.

In the $Ti_{1-2x}Cr_xNb_xO_{2-\delta}$ series the expansion of the unit cell is not isotropic, and as can be seen from Figure 2a there is a large increase in the size of the unit cell parameter *a* with reduction. The change in the unit cell parameter *c*, however, is much smaller going from the oxidized to the reduced state than that for *a*, Figure 2b. The negative deviation from Vegard's law shifts it toward the unit cell size of the oxidized sample, until in the $Cr_{0.5}Nb_{0.5}O_2$ the *c* parameter in the reduced sample is actually lower than that in the oxidized sample.

The link between the degree of reduction with the evolution of the unit cell parameter of the main, rutile phase, can be seen in Figure 2. The difference between the samples with the largest degree of reduction, $x = 0.1$ and 0.2, and those with the least amount of reduction, $x = 0.3-0.5$, indicates a complex interplay of a number of factors: (1) the increase in ionic radii of the cations with reduction, where the ionic radius of Ti^{3+} is 0.67 Å compared to 0.60 Å for Ti^{4+}, and that of Nb^{5+} is 0.64 Å compared to 0.68 Å for Nb^{4+}; (2) the increase in the average ionic radius as Ti^{4+} is substitution by larger Nb^{5+} and Cr^{3+}; and (3) the increasing metal−metal orbital overlap with increasing degree of reduction, and the evolution of the secondary phase (or shear planes) which incorporates oxygen vacancies.

This results in a nonlinear increase of the unit cell as a function of *x* in the reduced samples.

Previous studies have shown that as Nb_2O_5 is reduced to NbO_2 the increase in the metal−metal d-orbital overlap at the edge sharing octahedra produces shorter inter-metallic distance, going from 3.42 Å for Nb_2O_5[34] to 3.00 Å for NbO_2.[35] Further reduction to NbO increases the d-orbital overlap and reduces the Nb−Nb distance to 2.98 Å.[36,37] In Nb metal the Nb−Nb distance is 2.85 Å.[38] The edge sharing octahedra in the rutile structure are along the *c* axis (Figure 3); thus, as Nb^{5+} reduces to Nb^{4+} the metal−metal distance along the *c*-axis decreases. This would further indicate that Nb^{5+} is being reduced in preference to the Cr^{3+} ion.

Figure 5 shows the change in the *a* and *c* unit cell parameters of the rutile phases on going from oxidized to reduced states, Δa and Δc. It can be clearly seen that the increase in the *a* axis is significantly greater than in the *c* axis. Although initially the unit cell parameter *c* increases with oxygen loss, the negative slope of Δc as a function of composition shows that further cation substitution produces progressively smaller increases in *c*, up to $x = 0.3$ whereupon the unit cell parameter *c* decreases with reduction at $x = 0.4-0.5$. This would indicate that the cation substitution has a larger effect than an increase in the cation radius on reduction.

The significant increase in the volume of the unit cell (Figure 2c) is therefore primarily due to the expansion of unit cell parameter *a*, and the increase along this lattice as a function of *x* is larger for reduced samples. The *c*/*a* ratio in the reduced samples follows a trend similar to that for the oxidized samples (Figure 2 (d)), with the addition of a step between $x = 0.2$ and 0.3, due to a large increase in the M−O−M distance along the *a* axis with increasing cation substitution and decreasing amount of reduction at $x \geq 0.3$.

TEM. To understand the change in the structure on reduction and to explain additional peaks observed in the XRD pattern, TEM was performed on the pre-reduced samples.

HRTEM revealed the existence of a cluster of vacancies reminiscent of crystallographic shear (CS) planes in the reduced $Ti_{1-2x}Cr_xNb_xO_2$ series as shown in Figure 6. Magneli[39] recognized that in certain non-stoichiometric metal oxide systems, such as TiO_{2-x}, instead of continuous

(31) Hauf, C.; Kniep, R.; Pfaff, G. *J. Mater. Sci.* **1999**, *34*(6), 1287–1292.
(32) Andersson, S.; Collen, B.; Kuylenstierna, U.; Magneli, A. *Acta Chem. Scand.* **1957**, *11*(10), 1641–1652.
(33) Anderson, J. S.; Khan, A. S. *J. Less-Common Met.* **1970**, *22*(2), 219–&.
(34) Kato, K. *Acta Crystallogr., Sect/ B* **1976**, *32*(3), 764–767.
(35) Bolzan, A. A.; Fong, C.; Kennedy, B. J.; Howard, C. J. *J. Solid State Chem.* **1994**, *113*(1), 9–14.
(36) Andersson, G.; Magneli, A. *Acta Chem. Scand.* **1957**, *11*(6), 1065–1066.
(37) Bowman, A. L.; Wallace, T. C.; Yarnell, J. L.; Wenzel, R. G. *Acta Crystallogr.* **1966**, *21*, 843–&.
(38) Roberge, R. *J. Less-Common Met.* **1975**, *40*(1), 161–164.
(39) Magneli, A. *Nature* **1950**, *165*(4192), 356–357.

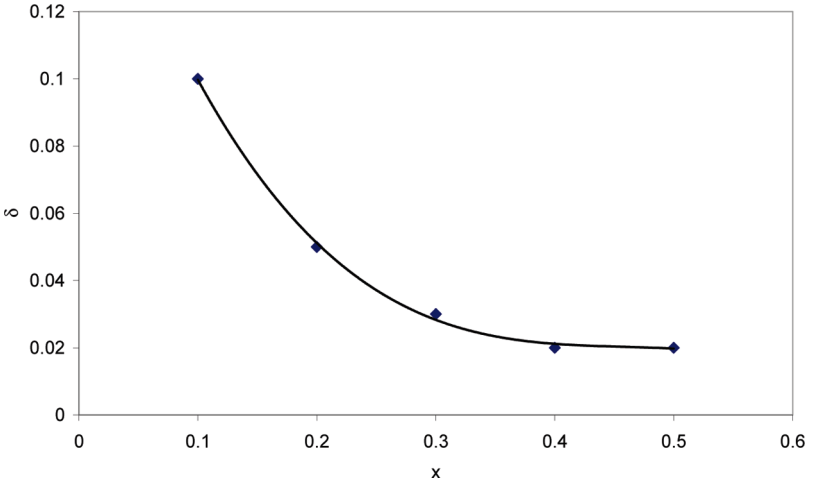

Figure 4. Change in δ as a function of x in $Ti_{1-2x}Cr_xNb_xO_{2-\delta}$.

Table 2. Refined Cell Parameters of the Secondary Phase in the Reduced Samples

nominal composition	space group (No.)	*a*	*b*	*c*	α	*β*	*γ*	*V*
$Ti_{0.8}Cr_{0.1}Nb_{0.1}O_{1.90}$	$I\bar{1}$ (2)	5.5872(6)	7.1086(6)	20.392(2)	67.767(9)	57.055(8)	108.766(8)	461.9(2)
$Ti_{0.6}Cr_{0.2}Nb_{0.2}O_{1.95}$	$R\bar{3}c$ (167)	4.974(1)		13.657(1)				292.7(1)
$Ti_{0.4}Cr_{0.3}Nb_{0.3}O_{1.97}$	$R\bar{3}c$ (167)	4.971(1)		13.690(1)				293.0(1)
$Ti_{0.2}Cr_{0.4}Nb_{0.4}O_{1.98}$	$R\bar{3}c$ (167)	4.956(1)		13.683(1)				291.0(5)
$Cr_{0.5}Nb_{0.5}O_{1.98}$	$R\bar{3}c$ (167)	4.947(1)		13.693(3)				290.2(1)

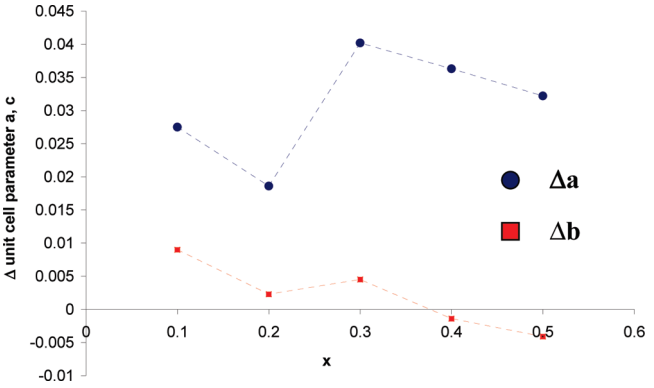

Figure 5. Δa and Δc unit cell parameters going from oxidized to reduced rutile structure.

solid solution formation, a series of closely related phases with similar formulae and structures exist in an oxide. In oxygen deficient rutile such as Ti_nO_{2n-1} ($n = 4, ..., 10$) or the $Ti_{1-2x}Cr_xNb_xO_2$ series, regions of normal rutile structure occur (Figure 6a), separated from each other by crystallographic shear (CS) planes (Figure 6b). Although close examination of the TEM images did not show any shift between consecutive atomic layers, which is a common feature in well formed CS planes, it may still indicate a presence of oxygen vacancy clusters, that is, the first stages towards the formation of a CS plane. The spacing between the planes is eight layers along the [101], corresponding to ~24 Å. As seen from the XRD data, the analogue phase is Ti_2O_3 for samples with $x = 0.2-0.5$, which although not a Magneli phase is a non-stoichiometric $TiO_{2-\delta}$ analogue corresponding to $(Ti_{1-x}Cr_xNb_x)_2O_3$. The Magneli phase with $n = 4$, corresponding to $(Ti_{0.8}Cr_{0.1}Nb_{0.1})_4O_7$, is only seen in the titania rich sample, with $x = 0.1$.

CS planes are thin lamellae of different structure and composition, and all of the oxygen deficiency is concentrated within these CS planes. With increasing reduction, the variation in stoichiometry increases the number of CS planes and decreases the block of rutile structure between adjacent planes. From the relative peak intensities of the main rutile phase to the secondary Ti_2O_3 type phase in the XRD patterns, the quantity of the Ti_2O_3 analogue is seen to decrease with increasing x, and is consistent with the TGA data showing a corresponding increase in the *average* cation oxidation state with increasing x.

In TiO_2, reduction of Ti^{4+} to Ti^{3+} or Ti^{2+} results in the formation of vacant oxygen sites, which are not randomly distributed but are located on certain planes within the crystal. To minimize the layers of vacant sites, condensation of the structure occurs, eliminating the vacancies and forming CS planes, where the octahedra share faces rather than edges as in the corresponding unreduced rutile regions.

The formation of shear planes may in part account for the nonlinearity observed in the TEC of the reduced samples with unit cell volume, as the thermal expansion of these shear planes may be significantly different from the bulk rutile structure; thus, further tests such as a high temperature XRD may need to be performed on the samples to explain the relationship between TEC and the unit cell parameters.

Thermal Expansion Data. The thermal expansion coefficient (TEC) is seen to decrease linearly with increasing x in the oxidized $Ti_{1-2x}Cr_xNb_xO_2$ series (Figure 7a) and is smaller for the reduced samples. The difference in the thermal expansion between the oxidized and the reduced samples is small, which is probably due to the retention of bulk rutile structure upon reduction. Thermal expansion is largest for $Ti_{0.8}Cr_{0.1}Nb_{0.1}O_{1.90}$ with 8.34×10^{-6} K^{-1}.

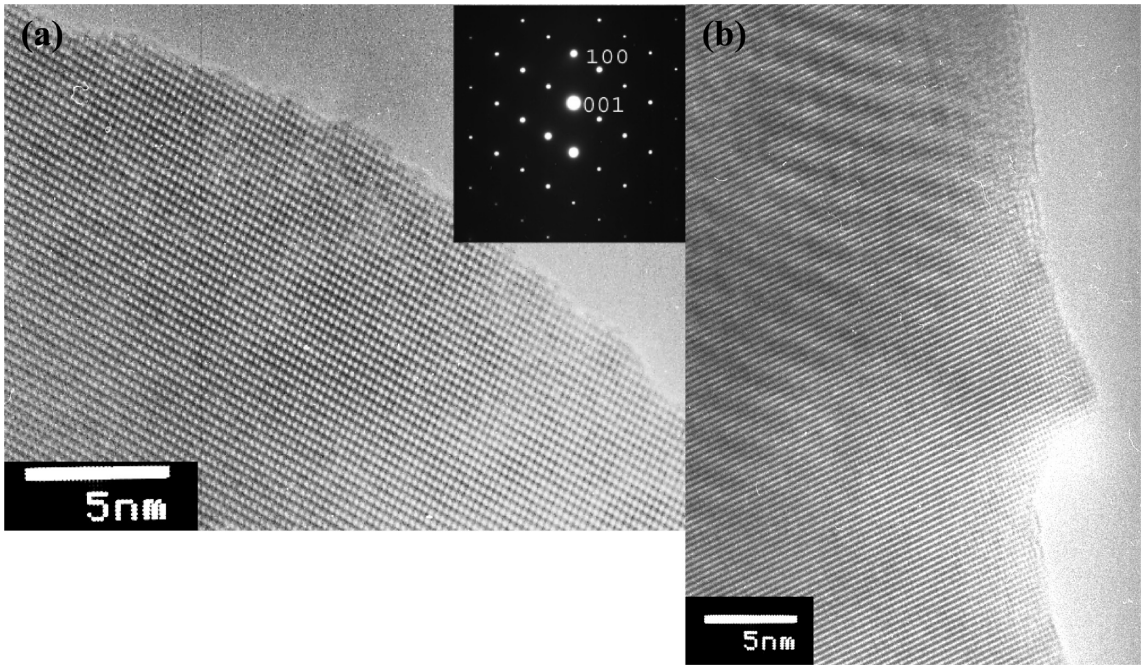

Figure 6. (a) HRTEM image corresponding to a view down the $[010]_t$ of a tetragonal rutile domain and its corresponding SAED pattern (inset) of $Ti_{0.2}Cr_{0.4}Nb_{0.4}O_2$, (b) HRTEM image of an oxygen deficient domain, recorded on a different area of the same crystal, of Figure 5a, and in the same direction, showing crystallographic shear planes of $Ti_{0.2}Cr_{0.4}Nb_{0.4}O_2$.

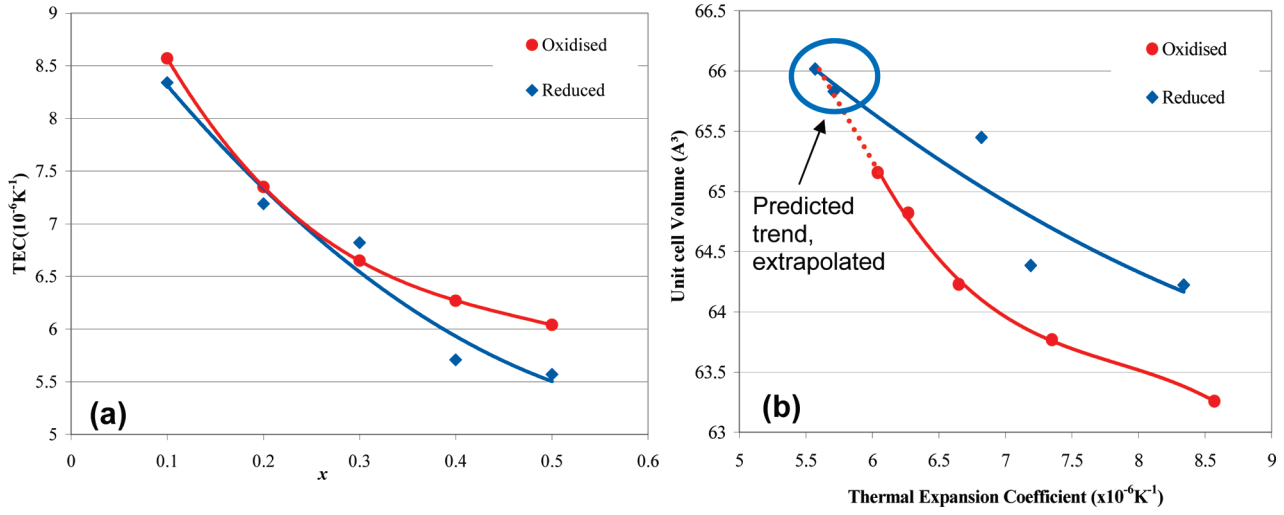

Figure 7. (a) Change in thermal expansion coefficient with x in the $Ti_{1-2x}Cr_xNb_xO_2$. (b) Thermal expansion coefficient as a function of unit cell volume for reduced and oxidized samples.

Small changes in the TEC with redox cycling is highly beneficial in high temperature applications such as the SOFC anode, leading to greater material stability and better mechanical properties.

The decrease in the unit cell volume is seen to correlate well with the increase in the thermal expansion coefficient, and relationship is noted in Figure 7b, with the smallest unit cell volume of 63.2 $Å^3$ and the largest thermal expansion of $8.57 \pm 0.05 \times 10^{-6}\,K^{-1}$, corresponding to $Ti_{0.8}Cr_{0.1}Nb_{0.1}O_2$, that is, $x = 0.1$. The least reduced samples, $x = 0.4-0.5$, highlighted by the blue circle (Figure 7b), follow the predicted trend line of the oxidized samples. Increasing the degree of reduction, however, seems to cause a deviation from the expected TEC, if it was directly related to the unit cell volume as suggested in Figure 7b, indicating that additional factors may be dominant in reduced samples, such as the presence of shear planes and non-stoichiometric TiO_x phases. As the expansion of the unit cell with doping is not isotropic, one would expect that the TEC is also not isotropic and may be significantly affected by the expansion of the a and c axes on reduction.

Although the TEC of these materials is lower than that of YSZ ($10.3 \times 10^{-6}\,K^{-1}$), the difference in the TEC between $Ti_{0.8}Cr_{0.1}Nb_{0.1}O_2$ and YSZ is less than that between NiO ($14.1 \times 10^{-6}\,K^{-1}$) or Ni metal ($16.9 \times 10^{-6}\,K^{-1}$) and YSZ in the Ni/YSZ cermet and is within the maximum 20% difference necessary for mechanical compatibility. Chemical compatibility, however, is yet to be investigated.

Table 3. Electronic Conductivities and Activation Energies of $Ti_{1-2x}Cr_xNb_xO_2$ in Air and 5% H_2/Ar

	σ (S cm^{-1}) in air at 900 °C	E_a (eV) heating (T °C range)	E_a (eV) cooling (T °C range)	σ (S cm^{-1}) 5% H_2/Ar at 900 °C	E_a (eV) heating (T °C range)	E_a (eV) cooling (T °C range)
$Ti_{0.8}Cr_{0.1}Nb_{0.1}O_2$	1.53×10^{-2}	1.07 (900−680) 0.38 (560−230) Curve 680−560	1.05 (900−680) 0.37 (560−230) Curve 680−560	20.6	0.11 (530−180) 0.16 (900−530)	0.12 (530−180) 0.14 (900−530)
$Ti_{0.6}Cr_{0.2}Nb_{0.2}O_2$	1.53×10^{-2}	1.54 (900−640) 0.77 (640−250)	1.37 (900−640) 0.71 (640−900)	22.3	0.17 (280−580) 0.26 (580−900)	0.19 (400 −280) 0.21 (400 −900)
$Ti_{0.4}Cr_{0.3}Nb_{0.3}O_2$	1.65×10^{-2}	1.30 (900−750) 0.75 (300−750)	1.29 (900−750) 0.64 (750−300)	21.2	0.23 (900−250)	0.24 (900−250)
$Ti_{0.2}Cr_{0.4}Nb_{0.4}O_2$	1.53×10^{-2}	0.62 (900−250)	0.63 (900−250)	10.9	0.39 (900−635) 0.32 (635−280)	0.30 (900−635) 0.33 (635−280)
$Cr_{0.5}Nb_{0.5}O_2$	2.49×10^{-2}	0.66 (700−900) 0.55 (700−160)	0.60 (900−370)	6.3	0.41 (200−900)	0.43 (900−200)

Four-Terminal DC Measurements. Four-terminal DC measurements are commonly used to evaluate the total conductivity of the sample as a function of temperature and $p(O_2)$. The advantage of using this technique over AC Impedance is the ability to measure samples with very low resistances, and conductivity as a function of $p(O_2)$ provides valuable insight into the conduction mechanism.

Two approaches at fixed temperature are used in collecting the data, a dynamic approach, where the partial pressure changes gradually with time and the change in $p(O_2)$ is constantly monitored by an oxygen sensor, and a static measurement, where a mixture of gases with a desired $p(O_2)$ are used to give a number of stationary points across the $p(O_2)$ range of interest. Although the static measurements are considered to provide equilibrium data for the small number of $p(O_2)$ points, the dynamic measurement can provide a much wider range of data points and can yield a better picture of the dependence of conductivity upon $p(O_2)$ and may include extra information on the kinetics of conduction mechanism change, rapid step transitions, and possible titration point information. The nature of the dynamic technique is such that common problems arise during data interpretation, and ambiguity often occurs in the intermediate $p(O_2)$ region of 10^{-12} to 10^{-6} atm where true equilibrium is difficult to achieve. In the dynamic technique the rate of change in the $p(O_2)$ compared to the kinetics of the sample under measurement determines whether true thermodynamic equilibrium is achieved or approached.

Many materials, such as TiO_2 derivatives, are known for their very slow kinetics and complex conduction mechanisms characteriszd by a range of point defects, such as electrons, oxygen vacancies, and metal interstitials[40] at ambient and low $p(O_2)$ and metal vacancies at high $p(O_2)$.[41] Many studies have been carried out into the defect equilibrium in TiO_2, and comprehensive review articles cover this area.[42−44]

Kofstad's studies[40] on the oxygen partial pressure dependency of the TiO_2 rutile structure suggested that a simple defect model in which either the oxygen vacancies or interstitial titanium defects predominate is inadequate to account for nonlinearity, with either temperature or $p(O_2)$, of defect concentration. Kofstad[40] thus proposed that the defect structure must simultaneously comprise of both the doubly charged oxygen vacancies and interstitial titanium atoms, with three or four effective charges.

Doping TiO_2, with aliovalent ions, has also been well investigated; however, for the purpose of this study niobium[45−47] and chromium[48,49] are of importance. In chromium doped samples, oxygen vacancies, and mixed-valence chromium and titanium interstitials govern the defect equilibrium. In niobium doped TiO_2, defect disorder is governed by oxygen vacancies and electronic and ionic charge compensation of niobium. The defect chemistry of rutile niobium and chromium doped TiO_2 can therefore be considered to be complex, governed by multiple defect regimes across the $p(O_2)$ range. As a result of this complexity, a static $p(O_2)$ measurement would be preferable to a dynamic one, especially as true equilibrium is difficult to achieve below 1000 °C in TiO_2.[50]

Electronic Conductivity at Constant Atmosphere. *Air.* The members of the $Ti_{1-2x}Cr_xNb_xO_2$ series show very similar conductivities in air at 900 °C (Table 3); however, the Arrhenius plot (Figure 8) shows the difference in the activation energies (E_a) for conduction. For titanium rich samples the activation energies are $1.07-1.54 \pm 0.01$ eV at high temperatures and $0.38-0.77 \pm 0.01$ eV at lower temperatures, indicating two different processes, one between 900 and 650 °C, with $E_a > 1$ eV corresponding to the enthalpy of defect formation and migration, and one below ~650−700 °C, with $E_a < 1$ eV corresponding to the enthalpy of migration only. Commonly referred to as intrinsic and extrinsic conductivity regimes, this change in conductivity in the Arrhenius plot could also relate to an electronic phase transition; however, titania is

(40) Kofstad, P. *J. Less-Common Met.* **1967**, *13*(6), 635–638.
(41) Nowotny, M. K.; Bak, T.; Nowotny, J.; Sorrell, C. C. *Phys. Status Solidi B* **2005**, *242*(11), R88–R90.
(42) Nowotny, J.; Bak, T.; Nowotny, M. K.; Sheppard, L. R. *J. Phys. Chem. C* **2008**, *112*(2), 590–601.
(43) Nowotny, J.; Bak, T.; Nowotny, M. K.; Sheppard, L. R. *J. Phys. Chem. C* **2008**, *112*(2), 602–610.
(44) Nowotny, M. K.; Sheppard, L. R.; Bak, T.; Nowotny, J. *J. Phys. Chem. C* **2008**, *112*(14), 5275–5300.
(45) Sheppard, L. R.; Bak, T.; Nowotny, J. *J. Phys. Chem. B* **2006**, *110* (45), 22447–22454.
(46) Sheppard, L. R.; Bak, T.; Nowotny, J. *J. Phys. Chem. B* **2006**, *110* (45), 22455–22461.
(47) Sheppard, L. R.; Bak, T.; Nowotny, J. *J. Phys. Chem. C* **2008**, *112* (2), 611–617.
(48) Carpentier, J. L.; Lebrun, A.; Perdu, F. *J. Phys. Chem. Solids* **1989**, *50*(2), 145–151.
(49) Bak, T.; Nowotny, M. K.; Sheppard, L. R.; Nowotny, J. *J. Phys. Chem. C* **2008**, *112*(18), 7255–7262.
(50) Kofstad, P. Nonstoichiometry, diffusion, and electrical conductivity in binary metal oxides; Wiley-Interscience: New York, 1972; pp xi, 382.

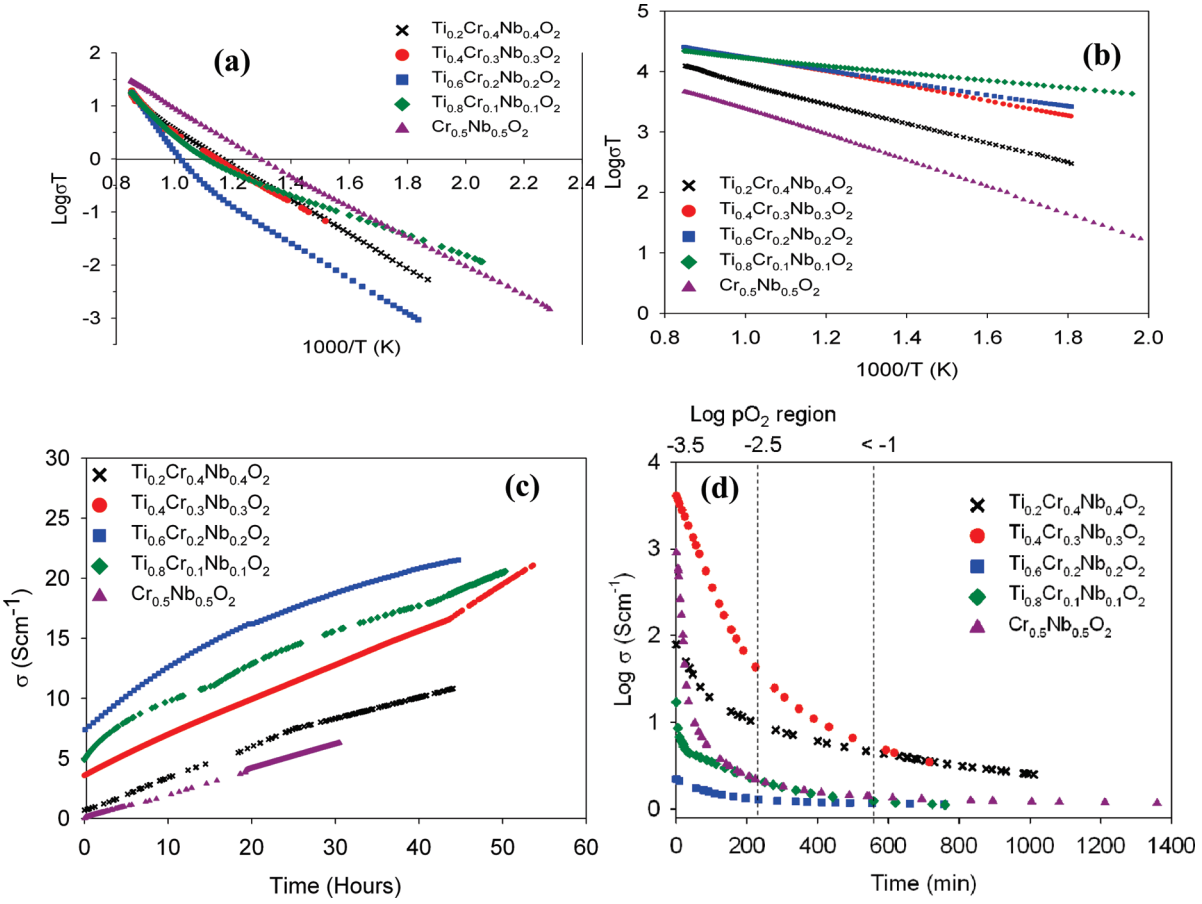

Figure 8. (a) Arrhenius plot of $Ti_{1-2x}Cr_xNb_xO_2$ for the conductivity measured in air. (b) Arrhenius plot of $Ti_{1-2x}Cr_xNb_xO_2$ for the conductivity measured in 5% H_2/Ar. (c) Change in conductivity with time at log $p(O_2)$ < −18.5 and 1173 K. (d) Change in conductivity with time at log $p(O_2)$ from < 3.5 to air and 1173 K.

one of the most heavily studied oxides, and the lower activation energy in air is generally agreed, in contrast to the disparity in the $p(O_2)$ studies, to be due to a small polaron hopping mechanism. $Ti_{0.2}Cr_{0.4}Nb_{0.4}O_2$ and $Cr_{0.5}Ti_{0.5}O_2$ shows no change in the activation energy across the entire measured temperature range (250−900 °C), and low activation energy of 0.55−0.66 ± 0.01 eV is seen for these samples. There is no difference in conductivity between the heating and cooling profiles of these materials, and no hysteresis is observed indicating phase stability and thermodynamic equilibrium.

5% H_2/Ar. Reduction of these materials increases the conductivity 1000-fold to > 20 S cm^{-1} for samples rich in titanium, dropping to 10 S cm^{-1} for $Ti_{0.2}Cr_{0.4}Nb_{0.4}O_2$ (Figure 8b), and the lowest conductivity observed for $Cr_{0.5}Nb_{0.5}O_2$ of 6.3 S cm^{-1}. The activation energies consistent with the band model for electronic conduction, as expected, are very low, 0.11−0.4 eV (Table 3), and increase both with temperature (> 550 °C) and with decreasing amount of Ti, once again suggesting that Ti^{4+} is reduced to Ti^{3+} and may be the cation primarily responsible for the electronic conduction. The increase of the activation energy for electronic conduction with increasing temperature in pure TiO_2 was ascribed by Blumenthal et al[51] to the decrease of the electron mobility with increasing temperature due to a scattering mechanism based on lattice vibration. In the Ti poor samples the incorporation of foreign cations would likewise be expected to disrupt the lattice and cause significant scattering. The lowest activation energy in this study was thus seen for samples with highest conductivities, namely, $Ti_{0.8}Cr_{0.1}Nb_{0.1}O_2$ with E_a = 0.11−0.16 eV when measured in 5% H_2/Ar.

All samples are characterized by slow reduction kinetics, and after 50 h of reduction in 5% H_2/Ar, equilibrium is still not achieved. Figure 8c shows the change in conductivity with time at $p(O_2) = 10^{-19}-10^{-20}$ atm at 900 °C, prior to the oxidation step in Figure 9. The reduction of these materials is slow, even with lowered densities of 70−85%, and the final conductivity equilibrium at 10^{-20} atm was not achieved. The conductivities of these samples when fully reduced would therefore be higher than those reported in this paper. Slow reduction kinetics are typical of the niobium and titanium based materials and indicate poor surface exchange rates or a low defect diffusion coefficient. Thus investigating the dependence of conductivity on $p(O_2)$ in these materials is difficult due to long time scales required, and in some samples geological time scales are required to reach an equilibrium at any one partial pressure. Hence, the data obtained from $p(O_2)$ measurements indicates a general trend rather than actual defect equilibrium.

(51) Blumenthal, R. N.; Kirk, J. C.Jr.; Hirthe, W. M. *J. Phys. Chem. Solids* **1967**, *28*(6), 1077–1079.

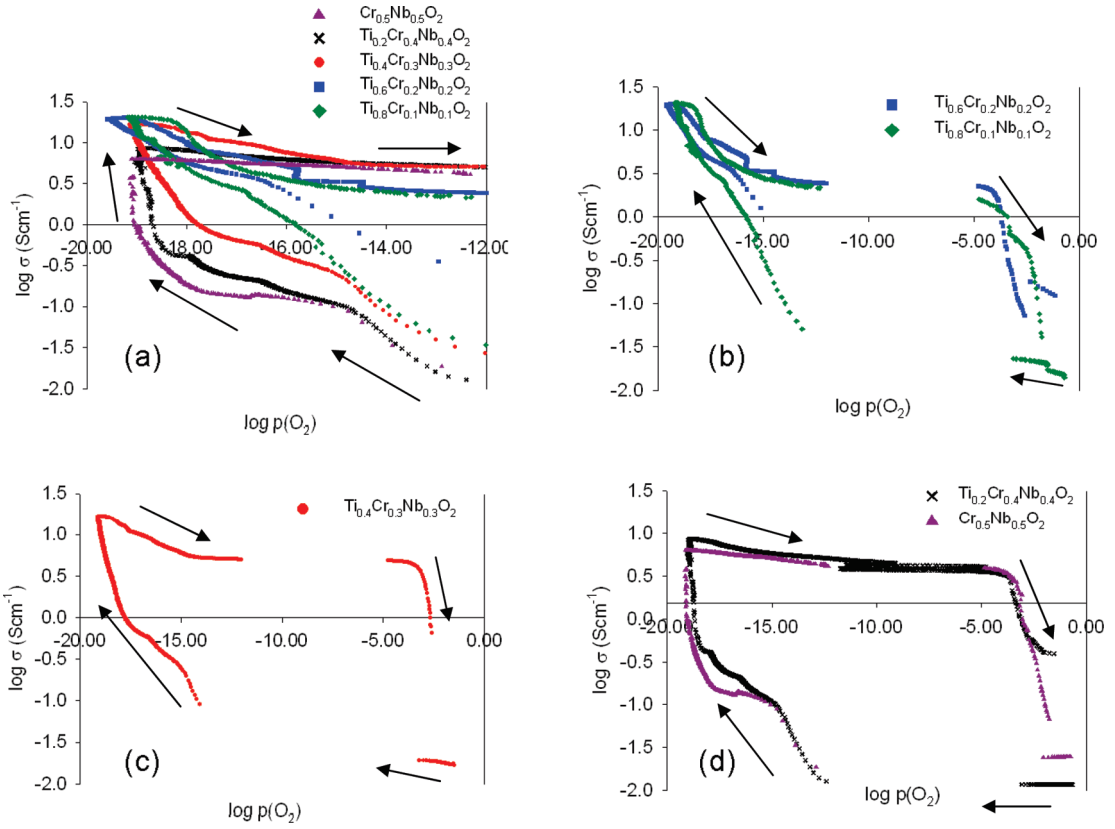

Figure 9. (a) log σ as a function of log $p(O_2)$ for $Ti_{1-2x}Cr_xNb_xO_2$. (b) log σ as a function of log $p(O_2)$ for $Ti_{0.2}Cr_{0.4}Nb_{0.4}O_2$ and $Cr_{0.5}Nb_{0.5}O_2$. (c) log σ as a function of log $p(O_2)$ for $Ti_{0.4}Cr_{0.3}Nb_{0.3}O_2$. (d) log σ as a function of log $p(O_2)$ for $Ti_{0.8}Cr_{0.1}Nb_{0.1}O_2$ and $Ti_{0.6}Cr_{0.2}Nb_{0.2}O_2$.

It is worth noting the steps in conductivity observed with holding time, possibly indicating different kinetic regimes. Defects formed at the surface diffuse into the bulk phase establishing a new equilibrium state. Fast defects, such as oxygen vacancies, exhibit high diffusion rates, whereas defects such as titanium vacancies are very slow.[52,53] Understanding of the chemical diffusion coefficient (D_{chem}) is necessary to ensure that a gas/solid equilibrium is reached and the defects are homogeneously distributed within the oxide specimen. For oxides that have a high degree of non-stoichiometry, such as TiO_2, D_{chem} shows a complex dependence on $p(O_2)$.

In these materials, the gradual increase in conductivity with time indicates that the equilibration process continues at a constant but very slow rate and that the gas/solid equilibrium is not established. As a result of such slow redox kinetics, the dynamic measurements of conductivity as a function of $p(O_2)$ in the next section cannot at any stage be considered to be equilibrium values, including the end points of the scan, which have had >50 h of equilibration time at a set $p(O_2)$.

Electronic Conductivity as a Function of $p(O_2)$. Typically the reduction step in the dynamic $p(O_2)$ experiment at $p(O_2) < 10^{-15}$ atm is difficult to control precisely and reproducibly by utilizing a needle valve without considerable experience, and on reduction often the rapid change in $p(O_2)$ with time is characterized by well-scattered data points. However, in this set of experiments the reduction region of 10^{-15} to 10^{-20} atm $p(O_2)$ was especially well controlled utilizing a fine needle valve and took up to 50 h to traverse, which although would be more than sufficient for equilibration of a large range of samples it is not sufficient for these materials. The oxidation stage is a more controllable step, and as such an average scan requires more time to complete, in this case up to 100 h to traverse the full $p(O_2)$ range, as seen in Figure 10.

The electronic conductivity of the $Ti_{1-2x}Cr_xNb_xO_2$ series can be separated into three similarly behaving groups of materials and is linked to composition (Figure 9). $Ti_{0.2}Cr_{0.4}Nb_{0.4}O_2$ and $Cr_{0.5}Nb_{0.5}O_2$ are very similar materials and can be considered to be TiO_2 doped $Cr_{0.5}Nb_{0.5}O_2$. $Ti_{0.8}Cr_{0.1}Nb_{0.1}O_2$ and $Ti_{0.6}Cr_{0.2}Nb_{0.2}O_2$ are at the other end of the compositional range, can be considered as TiO_2 rich phases with cation substitution, and will be treated as a group. The $Ti_{0.4}Cr_{0.3}Nb_{0.3}O_2$ solid solution is the intermediate phase and displays conductivity characteristics between the titanium rich and titanium poor compositions. The different kinetic profiles of these materials indicate a difference in defect types and rates of formation.

The slow kinetics in these materials are evidenced by a large hysteresis between reduction and oxidation steps. The size of the hysteresis, in spite of the long run times, indicates that the samples are far from equilibrium and that static $p(O_2)$ measurements of considerable duration would be required to determine a true $p(O_2)$ dependence.

(52) Nowotny, M. K.; Bak, T.; Nowotny, J. *J. Phys. Chem. B* **2006**, *110* (33), 16292–16301.
(53) Nowotny, M. K.; Bak, T.; Nowotny, J. *J. Phys. Chem. B* **2006**, *110* (33), 16302–16308.

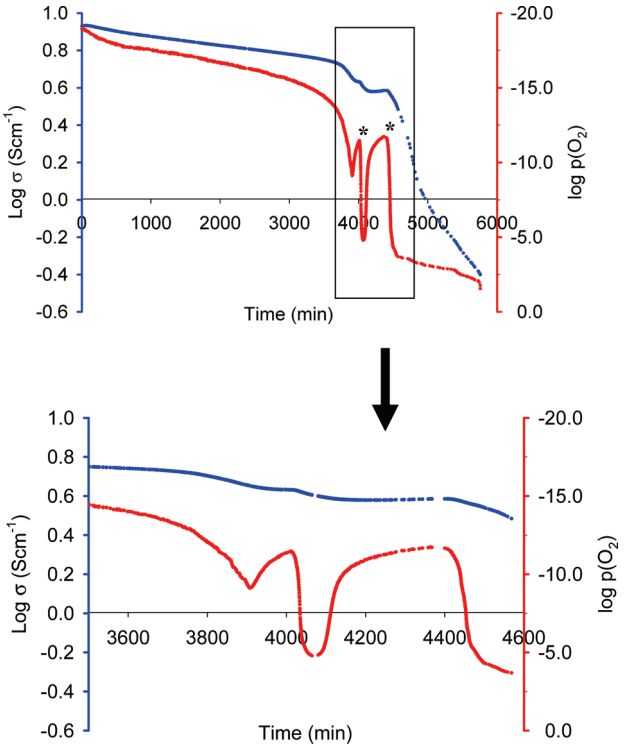

Figure 10. log $p(O_2)$ (red) and log σ (blue) as a function of time for $Ti_{0.2}Cr_{0.4}Nb_{0.4}O_2$. * shows the stage at which the needle valve was opened further.

However, as is demonstrated in Figures 8c,d and 10, the time scales for each point would have to be weeks and possibly months for true thermodynamic equilibrium to be reached.

The slow kinetics may be directly linked to the shear structure formation with oxygen loss as seen in the TEM micrographs. The shear defects are large structural rearrangements, which incorporate oxygen vacancies and titanium interstitials and have slow kinetics, as evidenced by the slow redox behavior.

After reduction, the samples displayed a high degree of stability to re-oxidation and none of the samples returned to their original conductivity in air after >50 h of equilibration time in atmospheric conditions. Figure 8d indicates that any structural changes and defect formation occurring during reduction, such as shear defects, may be "semi-permanent". Thus either higher temperatures or higher $p(O_2)$ regimes may be required to remove these structural defects.

The overall size of the hysteresis, as seen in Figure 9a, increases with decreasing titanium content and would be consistent with Ti^{4+} reduction determining the conductivity. Ti^{4+} is significantly easier to reduce than either Nb^{5+} or Cr^{3+}; hence, faster redox kinetics would decrease the hysteresis in the redox cycle. The degree of hysteresis shows distinct regimes for all samples, at high $p(O_2)$, $>10^{-4}$ atm, intermediate $p(O_2)$, 10^{-5} to 10^{-15} atm, and low $p(O_2)$, $<10^{-15}$ atm.

$Ti_{0.8}Cr_{0.1}Nb_{0.1}O_2$ and $Ti_{0.6}Cr_{0.2}Nb_{0.2}O_2$. The titanium rich group, $Ti_{0.8}Cr_{0.1}Nb_{0.1}O_2$ and $Ti_{0.6}Cr_{0.2}Nb_{0.2}O_2$, shows similar $p(O_2)$ dependence (Figure 9b), and in these materials the reduction and the oxidation reactions show higher degree of reversibility than other samples in the series. The hysteresis between 10^{-20} and 10^{-16} atm is small for both these samples, indicating faster redox kinetics than at high $p(O_2)$, and therefore a different defect dependency exists in this regime.

The gradient of the slope is only clearly evident for $Ti_{0.8}Cr_{0.1}Nb_{0.1}O_2$ and is $-1/4$, consistent with $Ti_i\cdots$ as the majority point defect in oxygen deficient TiO_2 in this partial pressure range and at this temperature.[54] This recent DC conductivity work on high purity single crystal TiO_2 by Lee and Yoo shows that there are actually three point defect regimes in the measured partial pressure range used in this study.[54]

In the intermediate partial pressures of oxygen, 10^{-4} to 10^{-15} atm where the degree of hysteresis is at its most pronounced in our experiments, $Ti_i\cdots$ is the dominant point defect in TiO_2, indicating that $Ti_i\cdots$ is also the dominant point defect in this regime for the titanium rich group and that the four plus interstitial cation formation has the most sluggish kinetics as you would expect.

At high $p(O_2)$, $>10^{-4}$ atm, the dominant point defect is also expected to be oxygen vacancies as for TiO_2, but this is further complicated by the apparent switch from p-type to n-type conductivity from thermoelectric power measurements[55] carried out on TiO_2, and even modest doping would be expected to significantly affect the defect concentrations near stoichiometry.[56]

Although step changes and variation in the slopes are seen in different $p(O_2)$ regions for both of these samples (Figure 9b), these are mainly governed by kinetics at these points, and as has been shown earlier, the redox kinetics in these materials are variable.

Step changes seen in the reduction and the oxidation step may be indicative of phase transition linked with the formation and destruction of shear defects. During re-oxidation, the conductivity of $Ti_{0.8}Cr_{0.1}Nb_{0.1}O_2$ is very similar to the pre-reduced sample, and this phase demonstrates the fastest and most reversible redox kinetics out of all the samples.

The "titration" point for complete re-oxidation is at $\sim10^{-4}$–10^{-3} atm as for other samples, and after the complete redox cycle the conductivity of $Ti_{0.6}Cr_{0.2}Nb_{0.2}O_2$ in air is lower than that of the pre-reduced material. This is uncharacteristic of these and other materials and may indicate that the sample had metastable defects remaining from the high temperature synthesis.

$Ti_{0.2}Cr_{0.4}Nb_{0.4}O_2$ and $Cr_{0.5}Nb_{0.5}O_2$. The largest hysteresis in the series is observed between the oxidation and the reduction steps (Figure 9d) for both $Ti_{0.2}Cr_{0.4}Nb_{0.4}O_2$ and $Cr_{0.5}Nb_{0.5}O_2$ and may indicate that the "titration" points for the oxidation and the reduction reactions are shifted. During reduction, the oxidized samples showed no change in conductivity up to $p(O_2)$ $\sim10^{-4}$–10^{-5} atm,

(54) Lee, D. K.; Yoo, H. I. *Solid State Ionics* **2006**, *177*(1–2), 1–9.
(55) Baumard, J. F.; Tani, E. *Phys. Status Solidi A* **1977**, *39*(2), 373–382.
(56) Hoshino, K.; Peterson, N. L.; Wiley, C. L. *J. Phys. Chem. Solids* **1985**, *46*(12), 1397–1411.
(57) Sugiyama, K.; Takeuchi, Y. *Z. Kristallogr.* **1991**, *194*(3–4), 305–313.

though with >10 h holding time some change should be observed, and this again may indicate geological time scales needed for equilibration or a titration point to induce rapid change. The following $p(O_2)$ region, $10^{-5}-10^{-15}$ atm, was traversed too fast, and no conclusion about the kinetics or conductivity dependence of the samples can be extrapolated from this region.

As a result of slow reduction kinetics, no reliable slopes can be derived during any stage of the redox cycle for reliable defect chemistry analysis and determination of D_{chem}; however, from the available data a number of possible phase transitions or shear defect formation can be seen in $Ti_{0.2}Cr_{0.4}Nb_{0.4}O_2$ and $Cr_{0.5}Nb_{0.5}O_2$. These are clearly shown in the reduction stage as step changes seen at $\sim 10^{-15}$ atm, 10^{-16} atm, and 10^{-18} atm. Once reduced these samples show a high degree of stability to any change in the $p(O_2)$. It is important to note that although the reduction step in this region was 15−20 h, these steps are not seen in the oxidation stage which took more than 50 h to traverse. For example, the oxidation step in the $p(O_2)$ that ranges from 10^{-19} to 10^{-14} atm for $Ti_{0.2}Cr_{0.4}Nb_{0.4}O_2$ took 60 h to traverse. This clearly demonstrates the irreversible nature of the formation of defects and that the equilibration time required for each point is different depending on the direction of the redox cycle. Thus the kinetics of the redox cycle are variable for these materials and supports the view that reaching the titration point is of higher significance than trying to achieve equilibrium via long measurements, when looking at change in these materials. During the oxidation step the conductivity changes little with increasing $p(O_2)$ up to 10^{-4} atm, and at this "titration" point rapid oxidation of the samples is indicated by a sudden drop in the conductivity.

Neither of these samples returned to their original, pre-reduction conductivity value in air, and the conductivity remained an order of magnitude higher after a complete redox cycle and re-oxidation in air. No further change in conductivity was observed after 48 h of equilibration in air at 900 °C.

Figure 10 shows the conductivity of $Ti_{0.2}Cr_{0.4}Nb_{0.4}O_2$ and $p(O_2)$ as a function of time, where what appears to be self buffering is observed across the $p(O_2)$ region of $10^{-12}-10^{-5}$ atm. The leak rate of oxygen was finely controlled with a needle valve, and at two points (marked with *) the oxygen leak rate was increased further for the atmosphere inside the sample chamber to reach $p(O_2)$ of 10^{-1} atm. This buffering behavior is unusual and has not been observed in other samples, and as such further study would be needed to explain the phenomenon. The step change in conductivity is seen during the "rapid" increase in $p(O_2)$ and again increasing during the "rapid" drop; however, the step changes are small, until the $p(O_2)$ reaches 10^{-4} atm. As can be seen from Figure 10, although the drop in $p(O_2)$ to 10^{-4} atm was fast, there is a clear lag in conductivity, and though appearing to be sudden, the time scale clearly shows that >16 h is required to reach the final point.

$Ti_{0.4}Cr_{0.3}Nb_{0.3}O_2$. $Ti_{0.4}Cr_{0.3}Nb_{0.3}O_2$ displays intermediate conductivity characteristics in both the conductivity values and the hysteresis, that is, redox kinetics, between the titanium rich and the titanium deficient groups discussed above, and is invariably linked to its intermediate composition in the solid solution series. The slope and step changes observed during the faster reduction step are not seen in a slower oxidation step (Figure 9d), once again indicating that redox kinetics are different for reduction and oxidation. Phase transitions are seen to occur at 10^{-16} atm and 10^{-18} atm during reduction, as for other samples, characterized by step like change in the conductivity. After the redox cycle, the conductivity remained an order of magnitude higher to pre-reduction and was not seen to change over 48 h of equilibration at atmospheric $p(O_2)$, again indicating "semi-permanent" structural changes.

Conclusion

Here we report an exciting discovery of highly redox stable TiO_2 based solid solution series, $Ti_{1-2x}Cr_xNb_xO_2$, that display mechanical and structural stability to reduction and re-oxidation. In addition, the high conductivity of these materials in reducing conditions opens up a wide range of applications.

There is no simple equilibrium equation to describe the defect equilibrium observed in the TiO_2 based rutile solid solution systems, but from the $p(O_2)$ dependencies observed there is a clear increase in the hysteresis with increasing x in the $Ti_{1-2x}Cr_xNb_xO_2$ series. The difficulty in establishing a true equilibrium and step change transitions rather than gradual changes occurring with time, indicating that the kinetics are a major contributor to the slopes observed, rather than the conduction mechanism, and as such longer studies are needed to truly understand the defect chemistry in these materials. Although the time scales over which these experiments were performed would be adequate for many materials, the ambiguity in the true equilibrium leads us to conclude that any additional analysis into the defect chemistry would be subject to large errors.

TEM studies showed that reduction of $Ti_{1-2x}Cr_xNb_xO_2$ produces crystallographic shear defects, which may incorporate oxygen vacancies and may explain poor redox cycling and slow redox kinetics. The final conductivity in air stabilized over 48 h shows that either higher temperatures and/or higher partial pressures of oxygen may be required to completely remove shear defects and fully re-oxidize samples after reduction.

The $Ti_{1-2x}Cr_xNb_xO_2$ solid solution series was investigated because they crystallize in a rutile structure, which may facilitate the reduction of niobium, and show high conductivity. With low Cr content, $x = 0.1-0.3$, the samples showed high conductivities of ~ 20 S cm^{-1} in reducing conditions. The samples, however, did not seem to reach the maximum conductivity after 50 h of equilibration at 900 °C in flowing 5% H_2/Ar; thus, their conductivity may be significantly higher than the values reported in this paper. Large hysteresis between reduction and oxidation steps and very slow redox

kinetics are characteristic in the conductivity of these materials.

Thermal expansion data shows a significant improvement on the Nb_2TiO_7 series,[15] with a maximum of $8.57 \pm 0.05 \times 10^{-6}$ K^{-1} (300−900 °C) observed for $Ti_{0.8}Cr_{0.1}Nb_{0.1}O_2$. The thermal expansion does not change significantly with reduction, making these materials ideal for high temperature applications involving different oxygen partial pressures, such as SOFC anode current collector. The high TEC indicates that $Ti_{0.8}Cr_{0.1}Nb_{0.1}O_2$ is more mechanically compatible with YSZ than Ni or NiO.

Although their high electronic conductivity and high TEC offer promise in current collecting applications, these materials require further study into their microstructure and interesting redox behavior, in particular $Ti_{0.8}Cr_{0.1}Nb_{0.1}O_2$ which demonstrated self-buffering in the region of 10^{-15}−10^{-5} atm.

$Ti_{1-2x}Cr_xNb_xO_2$ shows the required structural and mechanical redox stability, with high conductivity, making it a suitable candidate for further study for SOFC anode current collection applications. In addition their unusual electrochemical properties which include a large degree of stability at elevated temperatures and slow redox kinetics open a wide range of possibilities in other applications, such as thermal coatings and interconnected materials.